

ARCO-BO: Adaptive Resource-aware Collaborative Bayesian Optimization for Heterogeneous Multi-Agent Design

Zihan Wang¹, Yi-Ping Chen¹, Tuba Dolar¹, and Wei Chen^{1,*}

¹Department of Mechanical Engineering, Northwestern University, Evanston, IL, 60208

*Corresponding author

Abstract

Modern scientific and engineering design increasingly involves distributed optimization, where agents such as laboratories, simulations, or industrial partners pursue related goals under differing conditions. These agents often face heterogeneities in objectives, evaluation budgets, and accessible design variables, which complicates coordination and can lead to redundancy, poor resource use, and ineffective information sharing. Bayesian Optimization (BO) is a widely used decision-making framework for expensive black box functions, but its single-agent formulation assumes centralized control and full data sharing. Recent collaborative BO methods relax these assumptions, yet they often require uniform resources, fully shared input spaces, and fixed task alignment, conditions rarely satisfied in practice. To address these challenges, we introduce Adaptive Resource Aware Collaborative Bayesian Optimization (ARCO-BO), a framework that explicitly accounts for heterogeneity in multi-agent optimization. ARCO-BO combines three components: a similarity and optima-aware consensus mechanism for adaptive information sharing, a budget-aware asynchronous sampling strategy for resource coordination, and a partial input space sharing for heterogeneous design spaces. Experiments on synthetic and high-dimensional engineering problems show that ARCO-BO consistently outperforms independent BO and existing collaborative BO via consensus approach, achieving robust and efficient performance in complex multi-agent settings.

Keywords: Bayesian optimization, collaborative optimization, resource-aware optimization, multi-agent systems, task similarity.

1. Introduction

Modern scientific and engineering challenges increasingly demand coordinated efforts across multiple teams, disciplines, or organizations. Such collaboration is common in

domains like multi-fidelity design optimization [1], [2], materials discovery [3], [4], [5], and distributed manufacturing [6], [7], [8]. In multi-fidelity design, for instance, low-cost simulations provide broad exploration via faster/cheaper design evaluation, while high-fidelity experiments target promising candidates by focusing more on exploitation. In materials discovery, multiple laboratories may conduct experiments under different conditions or with distinct tools, each producing partial insights into a shared design space. In distributed manufacturing, facilities specialize in different stages of a product’s life cycle, each facing unique constraints and goals. These settings are a natural fit for a multi-agent design perspective [9], [10], where design agents (e.g., teams, labs, or models) contribute complementary, potentially heterogeneous information toward a common design objective. Heterogeneity can take many forms, including *function heterogeneity* when agents pursue related but distinct objectives, *budget heterogeneity* when resources are unequal, and *input-space heterogeneity* when exploration occurs in overlapping but not fully shared domains. In this work, we focus on collaboration rather than competition: agents coordinate to improve collective performance despite these differences. Figure 1 contrasts independent operation, where agents act in isolation, with collaborative operation, where agents exchange information through a consensus mechanism.

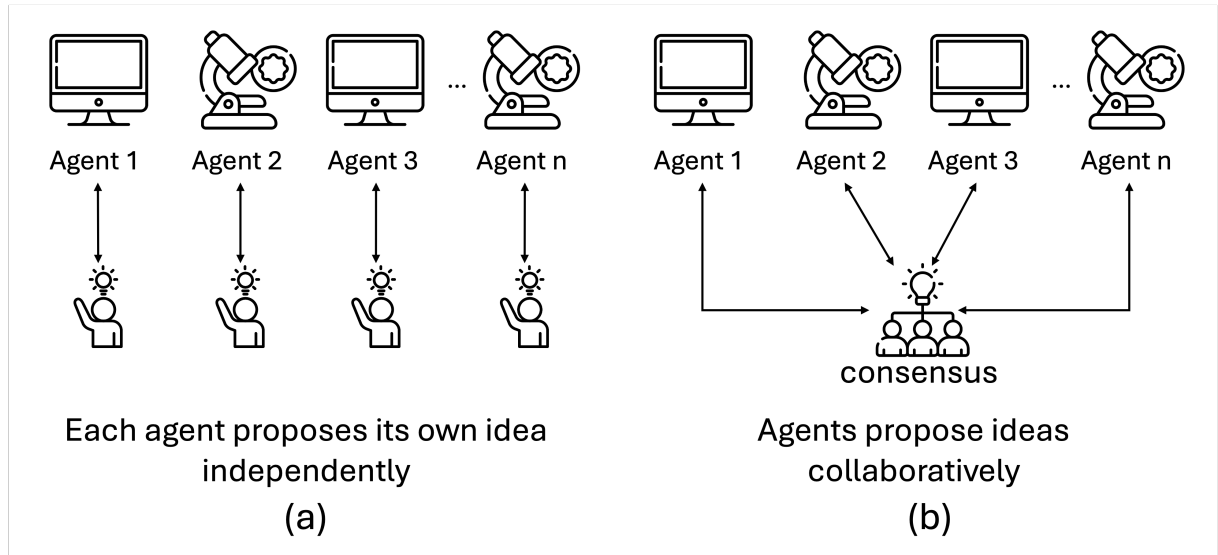


Figure 1: Conceptual illustration of multi-agent system. (a) Without collaboration, agents operate independently. (b) With collaboration, agents share information through consensus.

A variety of approaches have been developed for multi-agent design [11], [12], [13], [14], [15], [16], [17], [18], [19], [20], [21]. Distributed optimization [11], [12], [13] enables agents to solve a global problem via local updates and limited communication; methods such as distributed gradient descent and the Alternating Direction Method of Multipliers (ADMM) are widely used. Consensus algorithms [14], [15], [16], [17] align shared design variables through local interactions, often without centralized control. Game-theoretic frameworks [18], [19] model strategic agents and study equilibria and incentive-compatible mechanisms when cooperation cannot be assumed. Agent-based modeling

[20], [21] provides a flexible simulation framework for heterogeneous agents governed by decentralized decision rules. While effective in many settings, these methods rely on access to objectives or gradients and are not well suited for costly or heterogeneous tasks. Recently, multi-agent reinforcement learning (MARL) [22], [23], [24] has emerged as a data-driven approach that learns coordination directly from interaction, without explicit models of the environment or other agents. It suits dynamic or partially observable settings where handcrafted rules are impractical. However, many MARL methods emphasize reward maximization and fall short in sample efficiency and calibrated uncertainty, limiting their effectiveness in expensive design tasks. In practice, agents often face heterogeneous conditions. Coordinating these distributed efforts to achieve collective progress while minimizing redundancy is difficult, and exhaustive search or simple heuristics are often inefficient or brittle. In contrast, adaptive and resource-aware optimization approaches [25], [26], which guide evaluations based on feedback, uncertainty, and budget constraints, offer a promising path toward efficient and scalable multi-agent design.

Bayesian Optimization (BO) has been a popular effective adaptive learning framework for data-efficient decision-making in scenarios where evaluating objective functions is expensive [27], [28], [29]. BO leverages probabilistic surrogate models such as Gaussian Processes (GPs) [30] to estimate uncertainty and guides exploration through acquisition functions that balance exploration and exploitation to efficiently locate global optima with minimal samples. However, standard BO frameworks inherently assume a centralized, single-agent setup in which all evaluations and optimization decisions are controlled by a unified model operating over the entire design space. This assumption limits the applicability of traditional BO in distributed and collaborative environments where optimization tasks are performed by multiple agents or in a parallelized setup.

To overcome this limitation, collaborative BO [8], [31], [32] introduces a new paradigm for multi-agent design by enabling agents to share surrogate information and coordinate sampling decisions *without requiring centralized control or full data sharing*. The collaborative BO strategy proposed by [31] introduces constrained Gaussian process surrogates that enable agents to leverage informative evaluations discovered by high-performing collaborators. Rather than treating each agent’s optimization process in isolation, this method facilitates cross-agent knowledge sharing by selectively incorporating promising designs observed by others, subject to compatibility constraints. Another collaboration strategy proposed by [32] adopts a federated optimization paradigm, each agent trains its own model using its local data and then shares only certain parameters (like gradients or parts of the model) with others. By doing this, the agents work together to build a shared global model without directly sharing their raw data. More recently, consensus-based collaborative BO methods have been proposed [8] in which agents agree on their next-to-sample designs by sharing their local designs, but not design performances.

In parallel, emerging multi-source data fusion methods [33] offer an alternative paradigm for knowledge sharing through unified surrogate models. A representative example is the

Latent Variable Gaussian Process (LVGP) [34], which embeds discrete or high-dimensional variables into a continuous latent space to capture shared structures across heterogeneous tasks. In multi-fidelity optimization, LVGP has demonstrated strong potential for capturing shared structures and correlations across tasks or fidelity levels by implicitly learning task similarities through latent embeddings [2]. This enables effective information transfer across heterogeneous sources [35], thereby improving sample efficiency. Nevertheless, unlike collaborative BO frameworks that safeguard agent-level privacy by avoiding the exchange of true evaluation outcomes, LVGP requires access to both the input variables and the observed outputs from all agents in order to train a unified surrogate model. Additionally, the joint optimization of latent embeddings and hyperparameters may become computationally intensive as the number of agents increases, limiting LVGP’s scalability and applicability in many-agent systems.

While these advances mark notable progress in collaborative optimization, extending them to real-world multi-agent scenarios continues to pose substantial challenges. In particular, strong function heterogeneity across agents remains a hurdle for resource distribution in active learning under collaborative setup [36]. Beyond differing objectives, collaborative optimization often faces other forms of heterogeneity that further complicate coordination. In materials discovery, for instance, laboratories may pursue aligned optimization goals but operate under distinct process constraints, experimental budgets, and available input variables due to differences in equipment or protocols [37], [38]. In distributed manufacturing, concerns around data privacy and intellectual property frequently restrict the extent to which performance data or design specifications can be shared across organizational boundaries [39], [40], [41]. Multi-fidelity design presents yet another challenge, where computational agents can explore broad regions of the design space, while physical evaluations are limited to a smaller, costly subset [42]. These scenarios highlight three recurring and interdependent forms of heterogeneity that collaborative Bayesian optimization must confront: (1) heterogeneity in objective functions, (2) heterogeneity in evaluation budgets, and (3) heterogeneity in shareable input variables. However, existing work has mainly focused on limited function heterogeneity or privacy-aware coordination, without simultaneously addressing all three aspects in a unified framework.

In this paper, we propose Adaptive Resource-Aware Collaborative Bayesian Optimization (ARCO-BO), a framework specifically designed for multi-agent optimization in heterogeneous settings to handle the aforementioned limitations. As existing collaborative BO methods typically assume shared objectives, uniform resource budgets, or fully overlapping input spaces, ARCO-BO explicitly tackles three critical forms of heterogeneity: differing objective functions, asymmetric evaluation budgets, and partially shared input domains. To address these challenges, ARCO-BO introduces three key capabilities. First, it employs an adaptive, similarity-aware consensus mechanism that adjusts the degree of information sharing based on the alignment of surrogate models, enabling dynamic and selective collaboration among agents. Second, it implements a resource-aware

sampling strategy that schedules agent participation based on their available evaluation 137 budgets, promoting efficient and balanced exploration. Third, it enables collaboration 138 over partially shared input spaces, allowing agents to coordinate on common variables 139 while independently optimizing their private inputs. We evaluate ARCO-BO on both low- 140 dimensional illustrative examples and high-dimensional engineering problems, comparing 141 its performance to two baselines: (1) standard Bayesian optimization with independent 142 agents, and (2) conventional consensus-based collaborative BO with static update rules 143 [8]. Our results show that ARCO-BO consistently achieves superior design quality and 144 faster convergence across all tested scenarios. 145

The contributions of this work are summarized as follows: 146

- We introduce ARCO-BO, a novel framework for multi-agent Bayesian optimization 147 under heterogeneous settings, including function heterogeneity, asymmetric evalua- 148 tion budgets, and partially shared input spaces. 149
- We develop three key algorithmic components: a similarity-aware consensus mech- 150 anism for dynamic information sharing, a budget-aware sampling strategy to co- 151 ordinate evaluations based on remaining agent resources, and a partially shared 152 input model to handle heterogeneous design spaces across agents. 153
- We demonstrate that ARCO-BO consistently outperforms both independent optim- 154 ization and static-consensus baselines on synthetic benchmarks and high-dimensional 155 engineering design problems. 156

The remainder of this paper is organized as follows. Section 2 reviews the technical 157 background, including the existing Bayesian optimization and collaborative Bayesian op- 158 timization via consensus. Section 3 introduces the proposed ARCO-BO framework, de- 159 tailing its adaptive consensus mechanism, resource-aware sampling strategy, and support 160 for partially shared input spaces. Section 4 outlines the setup of numerical studies, includ- 161 ing evaluation metrics and computational configurations. Section 5 presents and analyzes 162 the results, comparing ARCO-BO to baseline methods across diverse multi-agent optim- 163 ization scenarios. Section 6 concludes the paper and discusses potential directions for 164 future research. 165

2. Technical Background 166

This section introduces the foundational concepts that motivate and inform our proposed 167 ARCO-BO. We begin with a review of BO, followed by its extension to collaborative 168 multi-agent settings via consensus-based Collaborative BO. These components highlight 169 the heterogeneity and coordination challenges that ARCO-BO is designed to address. 170

2.1 Bayesian Optimization

171

BO [27], [43], [44], [45] has emerged as a powerful framework for the global optimization 172 of expensive, black-box functions. In these settings, the objective function f is not ana- 173 lytically accessible and can only be evaluated through potentially noisy observations of 174 the form $y = f(\mathbf{x}) + \epsilon$, where $\epsilon \sim \mathcal{N}(0, \sigma^2)$ denotes independent Gaussian noise. The goal 175 is to identify the global minimizer of the function: 176

$$\mathbf{x}^* = \arg \min_{\mathbf{x}} f(\mathbf{x}), \quad (1)$$

with \mathbf{x} residing in a d -dimensional design space. A central challenge in BO lies in the high 177 cost of function evaluations, which severely limits the number of allowable queries. As 178 a result, exhaustive search strategies become impractical, and conventional optimization 179 methods often prove inefficient. BO addresses this challenge by leveraging a probabilistic 180 surrogate model to approximate the unknown objective function. This model guides 181 the selection of future query points in a way that strategically balances exploration of 182 uncertain regions with exploitation of areas likely to yield high performance. BO relies 183 on two fundamental components: a surrogate model (typically a Gaussian Process) and 184 an acquisition function that quantifies the utility of sampling each candidate point. 185

The Gaussian Process (GP) defines a distribution over functions and is characterized 186 by a mean function $\mu(\cdot)$ and a covariance function $k(\cdot, \cdot)$: 187

$$f(\mathbf{x}_{1:k}) \sim \mathcal{GP}(\mu(\mathbf{x}), k(\mathbf{x}, \mathbf{x}')). \quad (2)$$

Given an observed dataset $\mathcal{D} = \{(\mathbf{x}_i, y_i)\}_{i=1}^n$, the posterior distribution of f at a set of 188 new points $\mathbf{x}_{1:k}$ is: 189

$$f(\mathbf{x}_{1:k}) \mid \mathcal{D} \sim \mathcal{N}(\mu_n(\mathbf{x}_{1:k}), \Sigma_n(\mathbf{x}_{1:k}, \mathbf{x}_{1:k})), \quad (3)$$

where μ_n and Σ_n denote the posterior mean and covariance functions, respectively. 190

An acquisition function is a heuristic used to select the next sampling point. It takes 191 the GP posterior as input and balances exploration and exploitation. Common acqui- 192 sition functions [27], [29], [46] include Probability of Improvement (PI), Expected Improve- 193 ment (EI), Lower Confidence Bound (LCB), and Thompson Sampling (TS). We adopt EI 194 throughout this study due to its sensitivity to potential improvements and its efficiency 195 in converging to the optimum. 196

Assuming we have a minimization problem, the improvement utility function is: 197

$$u(\mathbf{x}) = \max(0, f^* - f(\mathbf{x})), \quad (4)$$

where f^* is the incumbent, i.e., the best (minimum) observed value so far. EI is formulated 198

as:

199

$$\begin{aligned}\alpha_{\text{EI}}(\mathbf{x}) &= \mathbb{E}[u(\mathbf{x}) \mid \mathcal{D}] \\ &= (f^* - \mu(\mathbf{x}))\Phi\left(\frac{f^* - \mu(\mathbf{x})}{\sigma(\mathbf{x})}\right) + \sigma(\mathbf{x})\phi\left(\frac{f^* - \mu(\mathbf{x})}{\sigma(\mathbf{x})}\right),\end{aligned}\quad (5)$$

where $\Phi(\cdot)$ and $\phi(\cdot)$ are the CDF and PDF of the standard normal distribution, and $\mu(\mathbf{x}), \sigma^2(\mathbf{x})$ are the GP posterior mean and variance. The next sampling point is chosen by maximizing $\alpha_{\text{EI}}(\mathbf{x})$. 200
201
202

2.2 Collaborative Bayesian Optimization via Consensus

203

As conventional BO is typically formulated for a single-agent setting, collaborative BO 204 205 206 207 208 generalizes the BO framework to accommodate these multi-agent scenarios by allowing agents to share information of the query samples to improve convergence efficiency. 209
210
211

In the consensus-based CBO framework proposed by Yue *et al.* [8], each agent $k \in \{1, \dots, K\}$ maintains its own surrogate model and acquisition function $U_k(\mathbf{x})$, selecting its candidate design point at iteration t as: 212
213
214
215

$$\mathbf{x}_k^{(t)} = \arg \max_{\mathbf{x}} \mathbb{E}_{\hat{f}_k | D_k^{(t)}} \left[U_k(\hat{f}_k(\mathbf{x})) \right], \quad (6)$$

where \hat{f}_k is the surrogate model fitted on agent k 's dataset $D_k^{(t)}$. 216

However, instead of immediately evaluating these proposals, the algorithm introduces a consensus step to enable collaboration. All agents' proposals $\mathbf{x}_k^{(t)}$ are aggregated via a consensus mechanism defined by a doubly stochastic matrix $\mathbf{W}^{(t)} \in \mathbb{R}^{K \times K}$. The updated, consensus-informed design for each agent is computed as the following: 217
218
219
220

$$\mathbf{x}_k^{(t, \text{new})} = \left[(\mathbf{W}^{(t)} \otimes \mathbf{I}_D) \mathbf{x}_C^{(t)} \right]_k, \quad (7)$$

where $\mathbf{x}_C^{(t)}$ concatenates the proposed designs from all agents, \mathbf{I}_D is the $D \times D$ identity matrix, \otimes denotes the Kronecker product, and $[\cdot]_k$ extracts the k -th block corresponding to agent k . The operation is illustrated in Figure 2, showing a two-agent system where each agent proposes a sample independently and then updates it through consensus, blending local decisions with input from the other agent to coordinate on shared design variables. 221
222
223
224

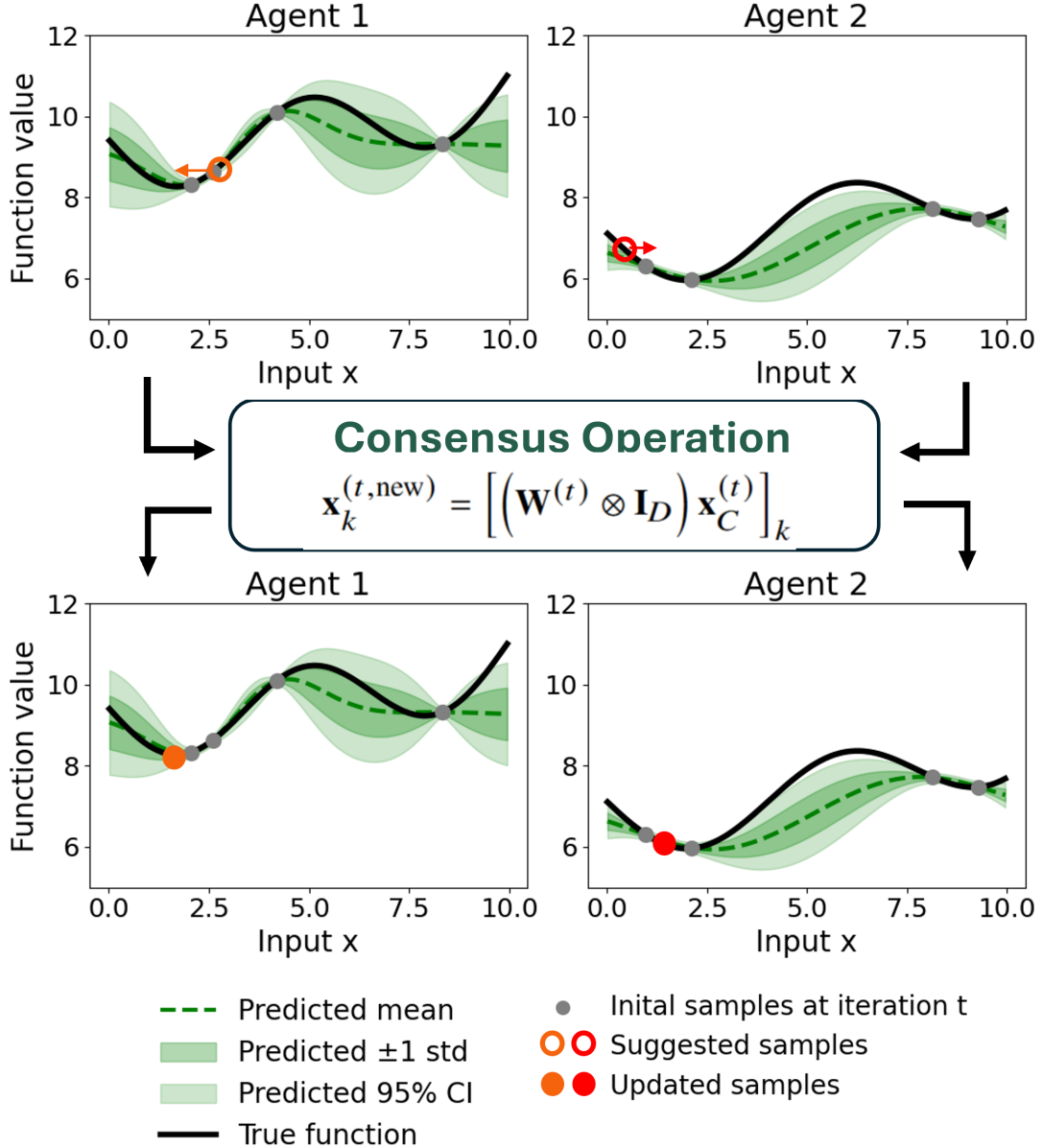


Figure 2: Consensus operation in collaborative Bayesian optimization. Agents first propose samples independently, then update their decisions via a weighted consensus based on the matrix $\mathbf{W}^{(t)}$.

Collaboration starts with full uniform averaging and gradually transitions towards [221](#) independent optimization. Specifically, the consensus matrix is initialized as: [222](#)

$$\mathbf{W}^{(0)} = \frac{1}{K} \mathbf{1}_{K \times K}, \quad (8)$$

where $\mathbf{1}_{K \times K}$ is a matrix of ones, representing equal weighting of all agents' proposals [223](#) when initialized. As optimization progresses, the consensus matrix evolves according to: [224](#)

$$\mathbf{W}^{(t+1)} = \mathbf{W}^{(t)} + \frac{1}{TK} \left[(K-1) \mathbf{I}_K - \mathbf{1}_{K \times K} \right], \quad (9)$$

where T is the total number of iterations. This update increases the diagonal elements w_{kk} [225](#) while decreasing the off-diagonal elements w_{kj} for $k \neq j$, effectively reducing the influence [226](#)

of other agents over time. In the limit, $\mathbf{W}^{(t)}$ converges to the identity matrix \mathbf{I}_K , enabling 227 agents to focus solely on their own objectives in later stages. The intuition behind this 228 transitional design is that in early optimization stages, each agent’s surrogate model is 229 trained on limited data and benefits from the information pooled from other agents. As 230 each agent accumulates more observations and constructs higher-quality surrogate models, 231 the optimization naturally shifts towards agent-specific refinement. 232

This consensus-based collaborative BO framework improves sample efficiency by co- 233 ordinating exploration across agents while preserving task-specific goals. However, it relies 234 on restrictive assumptions. It assumes agents optimize similar objectives with optima in 235 the same region, overlooking functional heterogeneity. When objectives are misaligned or 236 weakly correlated, uniform information sharing can cause negative transfer and slow con- 237 vergence. As shown in Figure 3, which depicts a three-agent system, Agents 2 and 3 are 238 highly correlated ($r = 0.77$), whereas Agents 1 and 3 are nearly uncorrelated ($r = -0.14$) 239 with distinct optima. The framework further assumes equal evaluation budgets, ignoring 240 resource asymmetries that lead to inefficient sampling and unbalanced contributions. It 241 also neglects partially shared input spaces, where coordination is possible only over sub- 242 sets of design variables. These limitations highlight the need for a more flexible, resource- 243 aware, and heterogeneity-adaptive framework for decentralized multi-agent design. 244

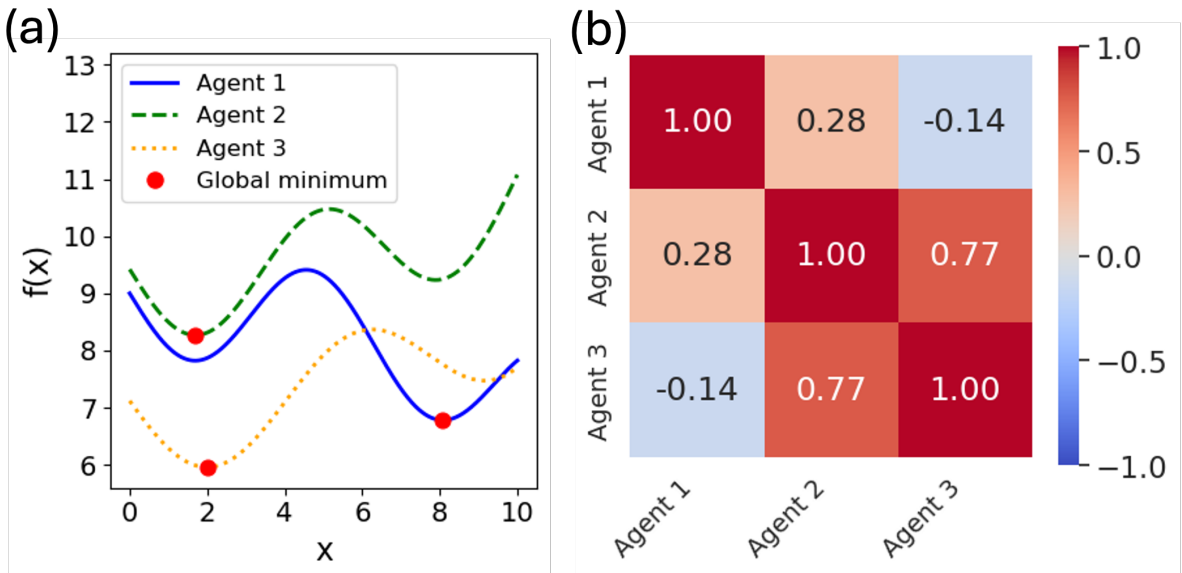


Figure 3: Illustration of function heterogeneity in a three-agent system. (a) Agent-specific objective functions $f_i(x)$, whose global minima lie in different regions of the domain. (b) Pairwise similarity shown as a correlation matrix.

3. Adaptive Resource-aware Collaborative Bayesian Optimization (ARCO-BO)

246

We propose an Adaptive Resource-aware Collaborative Bayesian Optimization (ARCO-BO) framework to enhance collaborative BO in the presence of task heterogeneity, resource disparity, and partially shared input spaces. ARCO-BO extends the consensus-based collaborative BO by introducing three key mechanisms: (1) Similarity and optima-aware dynamic consensus weighting, which promotes targeted knowledge exchange by adaptively weighting contributions from functionally related agents. (2) Budget-aware asynchronous sampling, which adjusts each agent's sampling frequency based on its evaluation budget, ensuring efficient resource utilization. (3) Partial input space sharing, which allows agents to collaborate even when their design spaces only partially overlap. The overall workflow of ARCO-BO is summarized in Algorithm 1.

Algorithm 1 ARCO-BO: Adaptive Resource-aware Collaborative Bayesian Optimization

Given: Initial data $\mathcal{D}_i = \{(\mathbf{x}_{ij}, y_{ij})\}_{j=1}^{n_i}$ for each agent $i \in \{1, \dots, K\}$, objective functions f_i , budgets B_i , search domain \mathcal{X}

Goal: Minimize each f_i under budget constraints

Initialize: Fit GP_i using \mathcal{D}_i for each agent. Let $B_{\max} = \max_i B_i$ and define update interval $\tau_i = \lfloor B_{\max}/B_i \rfloor$. Set iteration counter $t = 0$

While any $B_i > 0$ and $t < T$ **do**:

1. **Acquisition:** For agent i , if $t \bmod \tau_i = 0$ and $B_i > 0$, select:

$$\mathbf{x}_i^{(t)} = \arg \max_{\mathbf{x} \in \mathcal{X}} \alpha_i(\mathbf{x}; \text{GP}_i)$$

2. **Consensus:** Compute similarity matrix $\mathbf{S}^{(t)}$ and construct consensus weights $\mathbf{W}^{(t)}$
Update shared inputs:

$$\mathbf{x}_{\text{shared}}^{(t)} \leftarrow \mathbf{W}^{(t)} \cdot \begin{bmatrix} \mathbf{x}_{1,\text{shared}}^{(t)} \\ \vdots \\ \mathbf{x}_{K,\text{shared}}^{(t)} \end{bmatrix}$$

3. **Evaluation and Update:** For each agent i :

- Form input $\tilde{\mathbf{x}}_i^{(t)} = [\mathbf{x}_{\text{shared}}^{(t)}, \mathbf{x}_{i,\text{private}}^{(t)}]$
- Evaluate: $y_i^{(t)} = f_i(\tilde{\mathbf{x}}_i^{(t)})$
- Update data: $\mathcal{D}_i \leftarrow \mathcal{D}_i \cup \{(\tilde{\mathbf{x}}_i^{(t)}, y_i^{(t)})\}$
- Retrain GP_i , update budget: $B_i \leftarrow B_i - 1$

4. **Increment:** $t \leftarrow t + 1$

End while

Output: Final datasets \mathcal{D}_i and solutions $\hat{\mathbf{x}}_i$ (best in \mathcal{D}_i) for each agent

3.1 Similarity- and Optima-Aware Dynamic Consensus Weighting 257 258

Previous collaborative BO via consensus strategy [8] predominantly assumes uniform consensus weights, treating all agents as equally informative regardless of differences in their underlying objectives. While this assumption simplifies implementation, it is inherently limiting in heterogeneous settings where agents optimize related but non-identical tasks. Blindly aggregating information across dissimilar agents can degrade surrogate fidelity, introduce misleading guidance, and ultimately hinder optimization convergence. To address this limitation, ARCO-BO introduces a similarity- and optima-aware consensus mechanism that dynamically adjusts the influence of each agent based on both global functional similarity and local alignment of predicted optima. This approach ensures that information transfer is targeted and beneficial, promoting collaboration only where it enhances optimization performance. 259
260
261
262
263
264
265
266
267
268
269

Let K denote the number of agents, each maintaining a local GP surrogate model GP_k . To quantify inter-agent similarity, ARCO-BO computes behavior-based embeddings derived from each model's predictive mean over a shared input grid. Specifically, let $X_{\text{test}} \in \mathbb{R}^{N \times d}$ be a common test set sampled via Latin Hypercube Sampling within the design bounds. Following established heuristics in surrogate modeling and design of computer experiments, we set $N = 50d$, which provides sufficient resolution for model comparison in moderate dimensions [47], [48]. For each agent k , the predictive mean at each test input is computed to form a vector: 270
271
272
273
274
275
276
277

$$\boldsymbol{\mu}_k = \mathbb{E}[\text{GP}_k(X_{\text{test}})], \quad (10)$$

and its predicted minima location is determined by: 278

$$\mathbf{x}_k^* = \arg \min_{x \in X_{\text{test}}} \boldsymbol{\mu}_k. \quad (11)$$

If there happens to be more than one point with the same minimum value, we choose the one that appears first in the test set. 279
280

Stacking $\boldsymbol{\mu}_k$ across all agents yields the behavior matrix $\mathbf{M} \in \mathbb{R}^{K \times N}$, while stacking \mathbf{x}_k^* yields the minima matrix $\mathbf{X}^* \in \mathbb{R}^{K \times d}$. These matrices encode both global predictive behavior and local optimal regions for all agents. 281
282
283

The optima-aware similarity between agents i and j is then defined as: 284

$$s_{ij} = s_{ij}^{\text{Pearson}} \times s_{ij}^{\text{Proximity}}, \quad (12)$$

This multiplicative formulation ensures that high similarity is assigned only when both global trends and local optima are aligned. If either component is low, their product is suppressed, acting as a gating mechanism that avoids misleading collaboration. By enforcing joint agreement, the multiplicative form conservatively identifies agent pairs for 285
286
287
288

which information sharing is both reliable and beneficial. 289

s_{ij}^{Pearson} captures global similarity in functional behavior using the Pearson correlation coefficient, which measures the linear alignment between the predictive means of agents i and j . Let $\mu_{i,n}$ denote the n -th element of agent i 's predictive mean vector μ_i , and let 292

$$\bar{\mu}_i = \frac{1}{N} \sum_{n=1}^N \mu_{i,n}$$

be the average predictive value over the test set. The Pearson correlation coefficient is 293
then computed as: 294

$$\rho_{ij} = \frac{\sum_{n=1}^N (\mu_{i,n} - \bar{\mu}_i)(\mu_{j,n} - \bar{\mu}_j)}{\sqrt{\sum_{n=1}^N (\mu_{i,n} - \bar{\mu}_i)^2} \sqrt{\sum_{n=1}^N (\mu_{j,n} - \bar{\mu}_j)^2}}, \quad s_{ij}^{\text{Pearson}} = \frac{\rho_{ij} + 1}{2}. \quad (13)$$

This normalization maps the Pearson correlation from its original range of $[-1, 1]$ to 295
 $[0, 1]$, ensuring non-negative similarity scores that are compatible with weighting in the 296
consensus framework. 297

The second term, $s_{ij}^{\text{Proximity}}$, encodes minima proximity similarity, quantifying how close 298
the predicted optimal designs are: 299

$$s_{ij}^{\text{Proximity}} = \exp(-\lambda_p \|\mathbf{x}_i^* - \mathbf{x}_j^*\|^2), \quad (14)$$

where λ_p is a tunable hyperparameter that controls the sensitivity of the similarity score 300
to the distance between predicted minima. This exponential formulation ensures that 301
agents with nearby optima are weighted more strongly in the consensus. 302

In our implementation, we set λ_p such that $s_{ij}^{\text{Proximity}} = 0.1$ when the distance between 303
predicted optima is 10% of the input domain range $\Delta = \max(\mathbf{x}) - \min(\mathbf{x})$: 304

$$\lambda_p = \frac{-\ln(0.1)}{(0.1\Delta)^2}. \quad (15)$$

The 10% threshold is an empirically motivated choice based on initial experiments and 305
reflects a moderate tolerance for optima misalignment. However, this threshold can be ad- 306
justed depending on the problem context and desired sensitivity to proximity. In general, 307
 λ_p should be set to reflect the scale at which optima misalignment becomes detrimental 308
to collaborative inference. 309

Together, these yield a symmetric similarity matrix $\mathbf{S}^{(t)} \in \mathbb{R}^{K \times K}$ that captures both 310
global predictive consistency and alignment in locally optimal regions. To illustrate the 311
motivation behind our metric, Figure 4 shows how different function transformations 312
impact shape similarity and optima proximity. Each subplot compares a base function 313
 $f(x)$ (solid black) with a transformed variant (dashed gray). Transformations like vertical 314
shift and amplitude scaling (Figure 4a–b) preserve both shape and minimizer location, 315
resulting in high similarity. In contrast, sign flips (Figure 4c) or input shifts (Figure 4d–f) 316

degrade similarity by altering the function shape, the optima location, or both. These 317 examples highlight the need for a similarity metric that considers both global trends and 318 local optima. Our multiplicative formulation conservatively gates information sharing, 319 emphasizing collaboration only when both aspects are well aligned. 320

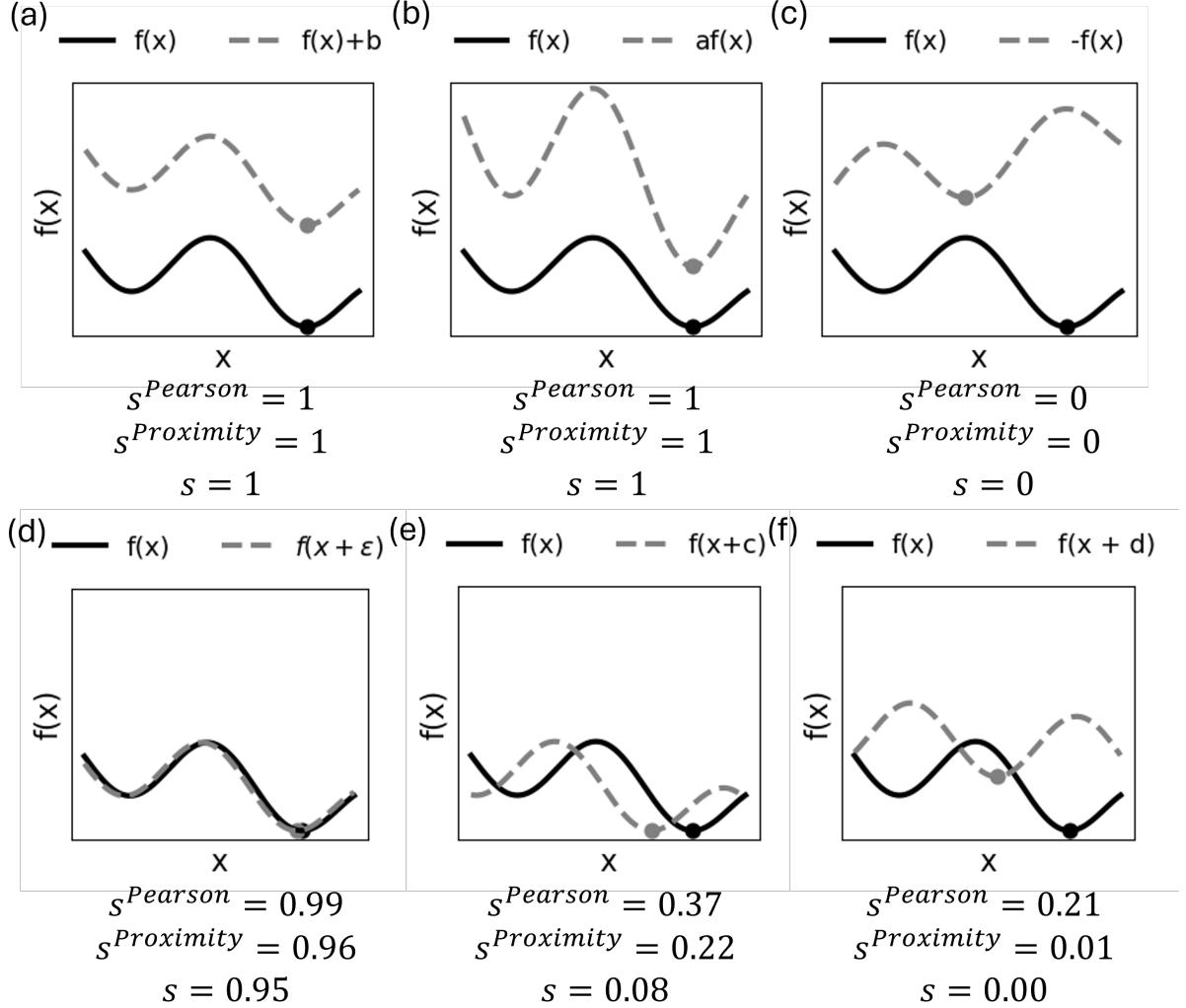


Figure 4: Illustration of function transformations and their impact on similarity. Each panel compares a base function $f(x)$ (solid black) with a transformed variant (dashed gray). (a) Vertical shift: $f(x) + b$ preserves both shape and minimizer location. (b) Amplitude scaling: $af(x)$ changes magnitude but keeps the same shape and minimizer. (c) Sign flip: $-f(x)$ inverts the shape and shifts the minimizer. (d) Small input shift: $f(x + \varepsilon)$ retains high similarity in both shape and minimizer location. (e) Moderate input shift: $f(x + c)$ preserves shape but misaligns the minimizer. (f) Large input shift: $f(x + d)$ leads to low shape and proximity similarity. Pearson correlation measures shape similarity, while proximity reflects alignment between minimizers.

To enable dynamic, similarity-aware collaboration, ARCO-BO constructs a time-varying consensus matrix: 321 322

$$\mathbf{W}^{(t)} = \gamma(t) \cdot \mathbf{S}^{(t)} + (1 - \gamma(t)) \cdot \mathbf{I}, \quad (16)$$

where $\mathbf{S}^{(t)} \in \mathbb{R}^{K \times K}$ is a non-negative similarity matrix, and \mathbf{I} is the identity matrix. The 323

scalar weighting function

324

$$\gamma(t) = \exp\left(-\frac{\alpha t}{T}\right) \quad (17)$$

controls the transition from early-stage collaboration ($\gamma(0) = 1$) to late-stage independent 325 optimization ($\gamma(T) \approx 0$). Here, T denotes the total number of BO iterations, and α is 326 a tunable hyperparameter that governs the decay rate. Larger values of α lead to faster 327 reduction in collaboration, while smaller values preserve stronger consensus for a longer 328 duration. 329

To ensure that $\mathbf{W}^{(t)}$ defines a valid consensus mechanism, it is normalized using Sink- 330 horn normalization [49], which iteratively rescales the rows and columns of a non-negative 331 matrix to make it doubly stochastic. The normalization is applied as: 332

$$\mathbf{W}^{(t)} \leftarrow \text{diag}(\mathbf{r})^{-1} \mathbf{W}^{(t)} \text{diag}(\mathbf{c})^{-1}, \quad (18)$$

where \mathbf{r} and \mathbf{c} are row and column scaling vectors, updated alternately until convergence. 333

This similarity- and optima-aware consensus strategy enables ARCO-BO to integrate 334 information across agents only when it is mutually beneficial, thereby enhancing sample 335 efficiency and improving convergence robustness in heterogeneous multi-agent optimiza- 336 tion settings. 337

3.2 Budget-aware Asynchronous Sampling

338

To realize the agent-specific sampling intervals τ_i introduced in of Algorithm 1, we incor- 339 porate a budget-aware asynchronous sampling mechanism. 340

In real-world collaborative optimization, agents often operate under heterogeneous 341 resource constraints. For instance, one agent might perform high-fidelity physical ex- 342 periments that are expensive and time-consuming, while another relies on low-fidelity 343 simulations that are faster and cheaper to evaluate. Similarly, some agents may be lim- 344 ited by equipment availability or operational cost, while others can afford frequent queries 345 due to lower evaluation overhead. Despite this variability, most existing collaborative BO 346 methods assume a uniform sampling rate, where all agents carry out the same number of 347 iterations or participate in collaborative updates at the same frequency. This assumption 348 can lead to inefficient use of resources, as fast agents are forced to wait for slower ones, and 349 costly evaluations are scheduled just as frequently as cheap ones. ARCO-BO addresses 350 this by introducing a budget-aware asynchronous sampling mechanism. Specifically, each 351 agent i is assigned a sampling interval τ_i based on its relative budget: 352

$$\tau_i = \left\lfloor \frac{B_{\max}}{B_i} \right\rfloor, \quad (19)$$

where B_i is the total budget for agent i and B_{\max} is the maximum budget among all 353 agents. This means agents with larger budgets sample more frequently, while those with 354 smaller budgets sample less often, helping them conserve their limited evaluations for the 355

most important points.

356

Agent i proposes a new point every τ_i iterations when it still has remaining budget. 357
Otherwise, it skips that iteration. This asynchronous sampling strategy allows each agent 358
to operate at a frequency proportional to its allocated budget, enabling more efficient 359
resource utilization and improved overall performance in collaborative optimization. 360

Currently, ARCO-BO assumes that the evaluation budgets B_i are fixed and known 361
in advance. However, the framework can be extended to accommodate dynamic budget 362
adjustment by periodically updating τ_i based on remaining budgets or runtime constraints. 363
Similarly, the model could be adapted to account for varying evaluation costs by defining 364
an effective budget in terms of cumulative cost rather than number of evaluations. We 365
leave these extensions for future work. 366

3.3 Partial Input Space Sharing

367

Building on our dynamic consensus mechanism of Algorithm 1, we now handle cases where 368
agents share only a subset of the design variables. 369

In many collaborative optimization problems, agents may have access to only a subset 370
of the global design variables due to factors such as unmeasurable parameters in ex- 371
periments or privacy constraints. As a result, their input spaces only partially overlap. 372
Conventional BO frameworks often assume a fully shared input space, which limits their 373
applicability in such heterogeneous settings. ARCO-BO addresses this by enabling partial 374
input space sharing within its consensus updates. Each agent's input is partitioned into 375
shared and private components: 376

$$\mathbf{x}_i = \begin{bmatrix} \mathbf{x}_{\text{shared},i} \\ \mathbf{x}_{\text{private},i} \end{bmatrix}, \quad (20)$$

where $\mathbf{x}_{\text{shared},i} \in \mathbb{R}^{d_s}$ are variables shared across agents, and $\mathbf{x}_{\text{private},i} \in \mathbb{R}^{d_p}$ are agent- 377
specific, such that $d_s + d_p = d$. Note that d_s and d_p may vary by agent. 378

During consensus updates, only the shared subspace is aggregated: 379

$$\mathbf{x}_{\text{shared}}^{(t+1)} = \mathbf{W}^{(t)} \mathbf{x}_{\text{shared}}^{(t)}, \quad (21)$$

while private variables remain unchanged:

380

$$\mathbf{x}_{\text{private},i}^{(t+1)} = \mathbf{x}_{\text{private},i}^{(t)}, \quad \forall i. \quad (22)$$

The final design combines both components:

381

$$\mathbf{x}_i^{(t+1)} = \begin{bmatrix} \mathbf{x}_{\text{shared},i}^{(t+1)} \\ \mathbf{x}_{\text{private},i}^{(t+1)} \end{bmatrix}. \quad (23)$$

This partial-sharing scheme ensures agents exchange only the overlapping dimensions, 382
preserving privacy of their private inputs while still leveraging joint exploration. 383

4. Evaluation Metrics

384

In this section, we introduce the quantitative metrics used to evaluate the performance 385 of multi-agent Bayesian optimization methods. In ARCO-BO, each of the K agents 386 performs one function evaluation per iteration, so one global iteration corresponds to up 387 to K parallel function calls. This execution model reflects a parallel deployment setting, 388 where agents operate independently and evaluate simultaneously without coordination. 389

Given that the objective is to identify the global optimum for each individual agent, 390 the evaluation metrics are designed to assess performance across all agents collectively. 391

1. **Normalized Final Regret.** To account for differences in objective function scales 392 across agents, we evaluate performance using the normalized final regret [50]: 393

$$\bar{r}^{\text{final}} = \frac{1}{K} \sum_{i=1}^K \frac{f_i(\mathbf{x}_i^*) - \min_{t=1,\dots,T} f_i(\mathbf{x}_i^{(t)})}{f_i^{\max} - f_i^{\min}}, \quad (24)$$

where $f_i(\mathbf{x}_i^*)$ is the known global minimum for agent i , and f_i^{\max} , f_i^{\min} denote the 394 maximum and minimum of the true function. A smaller value of \bar{r}^{final} indicates 395 closer proximity to the optimum. 396

2. **Normalized Area Under the Curve (AUC).** To evaluate early-stage conver- 397 gence behavior, we compute the normalized area under the averaged convergence 398 curve [51], which tracks the best objective value found so far over time. Specifically, 399

$$\overline{\text{AUC}} = \frac{1}{K} \sum_{i=1}^K \frac{1}{N} \sum_{t=1}^N \frac{\bar{f}_i^{(t)} - f_i(\mathbf{x}_i^*)}{f_i^{\max} - f_i^{\min}}, \quad (25)$$

where $\bar{f}_i^{(t)}$ is the mean of the best objective value found by agent i up to iteration 400 t , averaged across replicates, and N is the number of early-stage iterations. A 401 smaller $\overline{\text{AUC}}$ indicates faster convergence to the optimum during the initial phase 402 of optimization. In our test cases, we use $N = 0.1T$ to represent the early-stage 403 phase of optimization. 404

All experiments were performed on a workstation running Ubuntu 20.04, equipped 405 with an AMD EPYC 7413 processor (24 cores) and 64 GB of RAM. The code was imple- 406 mented in Python 3.9 and executed on the CPU. 407

5. Case Studies

408

In this section, we first present a 1D illustrative example demonstrating how our method 409 works differently in contrast to conventional collaborative BO via consensus when optim- 410 izing heterogeneous functions. Next, we demonstrate the effectiveness of the proposed 411

ARCO-BO method on a 2D example exhibiting three types of heterogeneity: task heterogeneity, resource disparity, and partially shared input spaces. This example highlights the advantages of ARCO-BO over applying separate BO independently to each agent. Finally, we evaluate ARCO-BO on two high dimensional engineering benchmarks: the borehole function (8D) and the wing weight function (10D). These engineering problems are widely used in surrogate-assisted optimization and test ARCO-BO’s ability to scale in terms of both consensus overhead and distributed sampling efficiency in higher dimensions.

It is important to note that although these benchmark functions are originally used as test cases for multi-fidelity designs [2], we treat each fidelity level as a separate agent task in this study, each with its own objective and ground truth, rather than treating the highest fidelity function as a ground-truth, and the objective is to identify the optimal solution for each agent simultaneously.

5.1 1D Illustrative Example

To evaluate the robustness and collaborative dynamics of ARCO-BO, we consider a multi-agent optimization problem based on variants of the Sasena function [52], where three agents each optimizes distinct but related functions with different global minimum locations. These variations emulate realistic heterogeneity arising from differences in modeling fidelity, operating conditions, or task formulations, which is common in engineering design and simulation. Details of the agent-specific functions, lower and upper bounds, budgets, and true optimal are provided in Table A1. Each agent begins with three randomly sampled initial evaluations, which are kept consistent across all compared methods to ensure a fair comparison.

In this example, all Gaussian process surrogate models use a squared exponential (RBF) kernel, with fixed lengthscale 0.5, signal variance 1.0, and Gaussian observation noise with variance 10^{-6} . Figure 5 illustrates the GP updates at the last iteration under three optimization strategies. Figure 5a shows a separate BO, where each agent optimizes independently without collaboration. While the predicted means generally align with the true functions, the models exhibit high uncertainty in unexplored regions. Figure 5b illustrates the behavior of an existing collaborative BO method based on uniform consensus, where agents share information equally regardless of task alignment. This uniform sharing often leads to incorrect collaboration, as conflicting information from agents with different objectives is combined without regard for compatibility. Consequently, agents are misled in their sampling decisions, resulting in suboptimal exploration and poor convergence. This issue is visually highlighted by the red boxes and arrows, which indicate significant deviations from the true optima. In contrast, Figure 5c shows the results of ARCO-BO, which adaptively reweights inter-agent influence based on task similarity and differences in optimal solution locations. The four heatmaps (Figure 6) depict the learned inter-agent weight matrix W , where each cell (i, j) is the weight agent i assigns to agent j . Because Agent 1’s optimum is far from those of Agents 2 and 3, their pair-

wise similarity is near zero; consequently ARCO-BO suppresses the cross-weights W_{12} 451 and W_{13} (and symmetrically W_{21} , W_{31}) toward zero. By contrast, Agents 2 and 3 are 452 similar, so ARCO-BO initially assigns cross-weights W_{23} and W_{32} to facilitate sharing; as 453 both agents approach their optima, these weights taper and W sharpens toward a near- 454 diagonal structure, evidencing reduced cross-agent influence and increasing self-reliance. 455 This targeted collaboration enables agents to focus sampling near their true optima while 456 avoiding misleading guidance from incompatible tasks. 457

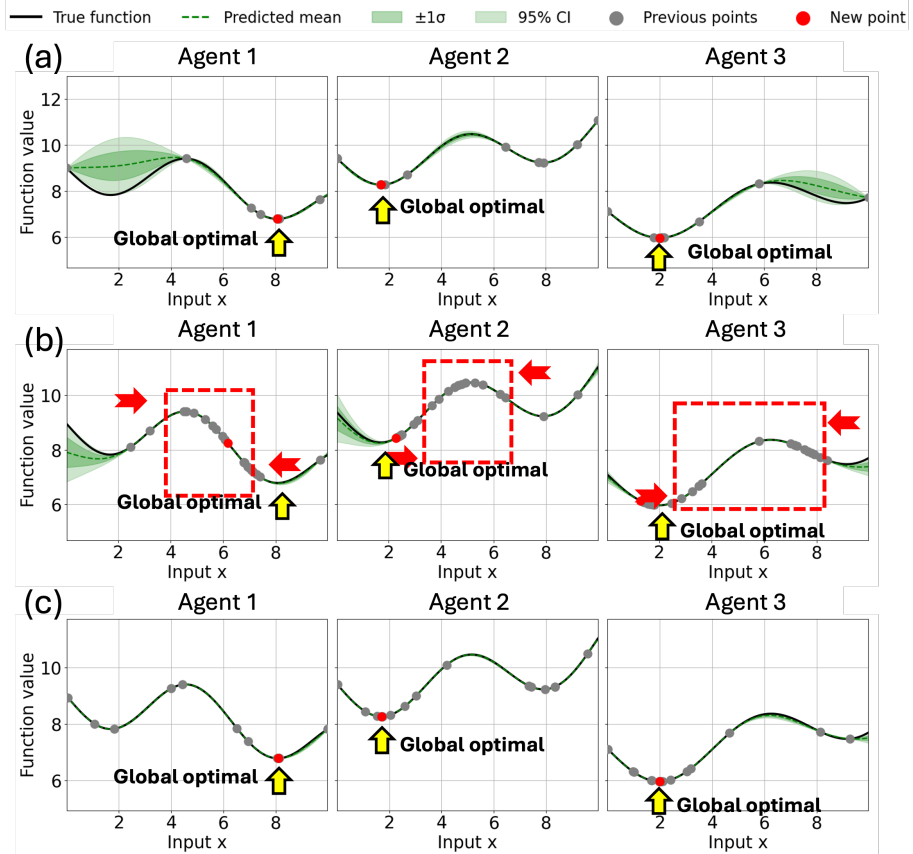


Figure 5: Comparison of surrogate model predictions across three optimization strategies at iteration 20 for three agents optimizing distinct variants of the Sasena function. (a) separate BO, (b) benchmark collaborative BO and (c) our proposed ARCO-BO.

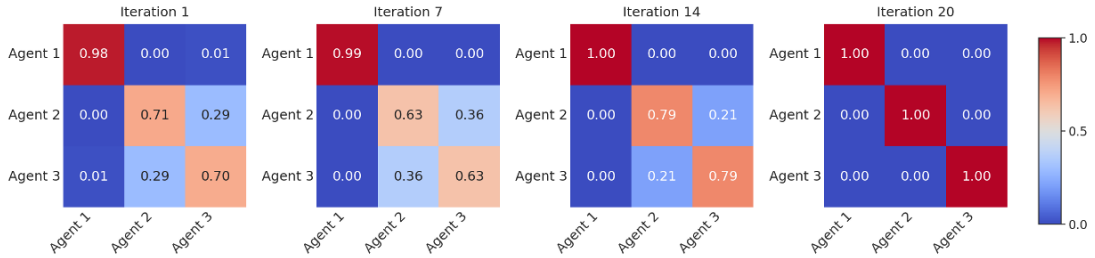


Figure 6: Progression of the learned inter-agent weights W under ARCO-BO at iterations 1, 7, 14, and 20.

Figure 7 further quantifies the benefits of ARCO-BO based on 50 independent replicates, each generated using different initial samples drawn for the agents. In the top row, 458 459

each plot shows the mean best function value (y^*) over iterations, comparing ARCO-BO 460 with conventional collaborative BO via consensus and separate BO. The results demon- 461 strate that ARCO-BO enables faster convergence to each agent’s optimum. In contrast, 462 the baseline collaborative BO fails to outperform separate BO and often does not reach 463 the true optima, due to overly strong information sharing that misguides agents with 464 divergent objectives. The bottom row shows the standard deviation of the best func- 465 tion values, indicating that ARCO-BO also achieves greater robustness in optimization 466 performance. To further assess performance, we compute the normalized AUC and the 467 normalized final regret, as summarized in Table 1. Both separate BO and ARCO-BO are 468 able to reach the global optima for all agents, while the baseline collaborative BO fails to 469 do so. Among all methods, ARCO-BO achieves the fastest early convergence, highlighting 470 the effectiveness of its adaptive and similarity-aware collaboration strategy. 471

Table 1: Normalized AUC and normalized final regrets for the 1D Sasena problem, reported as mean \pm standard deviation across 50 replicates.

Method	AUC	Final Regret
Separate BO	0.1623 ± 0.2048	0.0000 ± 0.0000
Benchmark CBO	0.1840 ± 0.1872	0.0483 ± 0.0790
ARCO-BO	0.1562 ± 0.2017	0.0000 ± 0.0000

Table 2: Normalized AUC and normalized final regrets for the 2D Ackley problem in three different scenarios, reported as mean \pm standard deviation across 50 replicates.

Scen.	Method	AUC	Final Regret
1	Separate BO	0.2784 ± 0.1483	0.0169 ± 0.0159
	Benchmark CBO	0.2050 ± 0.0870	0.0929 ± 0.0669
	ARCO-BO	0.2008 ± 0.0932	0.0145 ± 0.0158
2	Separate BO	0.2770 ± 0.1486	0.0143 ± 0.0159
	ARCO-BO	0.1992 ± 0.0933	0.0125 ± 0.0158
3	Separate BO	0.2784 ± 0.1483	0.0186 ± 0.0186
	ARCO-BO	0.1861 ± 0.0975	0.0145 ± 0.0158

5.2 2D Illustrative Example

We consider a multi-agent problem based on variations of the 2D Ackley function [53], a 473 widely used benchmark known for its numerous local minima and challenging non-convex 474 landscape. We design three scenarios to assess ARCO-BO’s capabilities: (1) agents have 475 the same evaluation budgets with both input variables fully shareable; (2) agents have 476 different evaluation budgets with both input variables shareable, simulating heterogeneous 477 resource availability; and (3) agents have the same budgets but only one input variable is 478

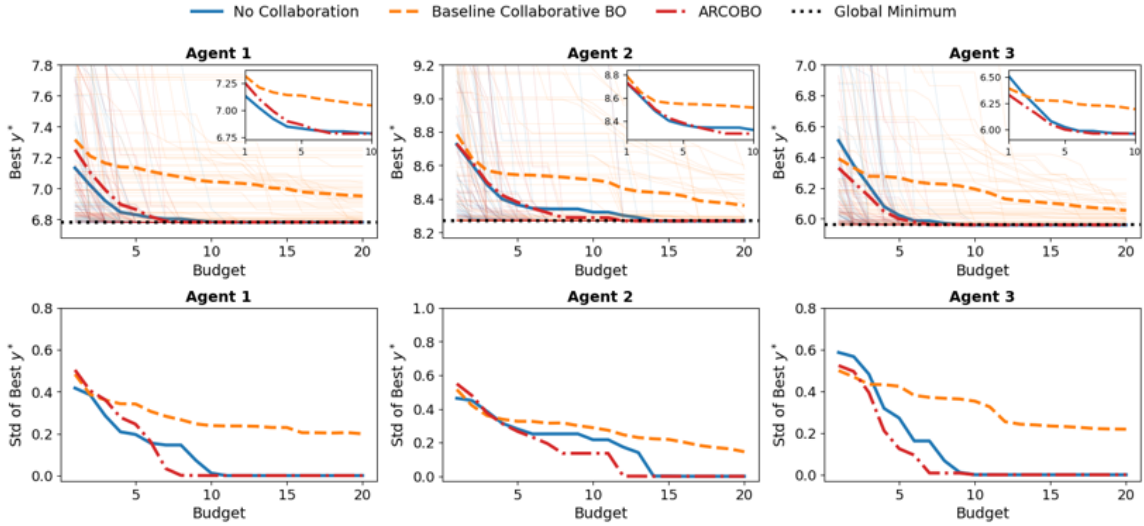


Figure 7: Convergence performance of ARCO-BO compared to baseline methods on the multi-agent Sasena problem, evaluated over 50 independent replicates.

shareable, reflecting partial input sharing constraints. In all cases, ARCO-BO is compared 479 against separate BO and, where applicable, a benchmark collaborative BO via consensus. 480

Detailed information about the six agents is listed in Table A2. In the second scenario, 481 agents 2, 3, and 6 are assigned only half of the original evaluation budgets to reflect 482 resource differences. Each scenario is evaluated across 50 independent replicates, and we 483 report both the normalized AUC and the normalized final regret for all agents (Table 2). 484 We use an RBF kernel with fixed lengthscale 0.5, signal variance 1.0, and observation 485 noise variance 10^{-6} . 486

In scenario 1 (Figure 8a), where agents have equal evaluation budgets and both input 487 variables are fully shareable, ARCO-BO achieves rapid convergence. Compared to the 488 benchmark collaborative BO, which often fails to converge to each agent’s local optimum 489 due to detrimental information transfer, ARCO-BO demonstrates clear advantages by 490 enabling agents to collaborate selectively only when it is mutually beneficial. 491

In scenario 2 (Figure 8b), where agents have different evaluation budgets but both 492 input variables remain shareable, ARCO-BO maintains robust optimization performance 493 despite the heterogeneous resource distribution. Notably, separate BO struggles under 494 this setting because agents with low budgets cannot adequately explore their objective 495 landscapes, which leads to the convergence on suboptimal solutions (agent 2, 3 and 6 496 in Figure 8b). In contrast, ARCO-BO utilizes knowledge transferred from higher-budget 497 agents to guide low-budget agents towards better solutions, leading to improvements in 498 convergence speed and final regret compared to baselines. 499

In scenario 3 (Figure 8c), where agents have the same budgets but only one input 500 variable is shareable, ARCO-BO continues to demonstrate its advantages over separate 501 BO. While partial input sharing limits the extent of collaboration, ARCO-BO’s adaptive 502 consensus mechanism ensures that agents only share useful and consistent information 503 along the shared dimensions. As a result, it still outperforms independent BO, which 504

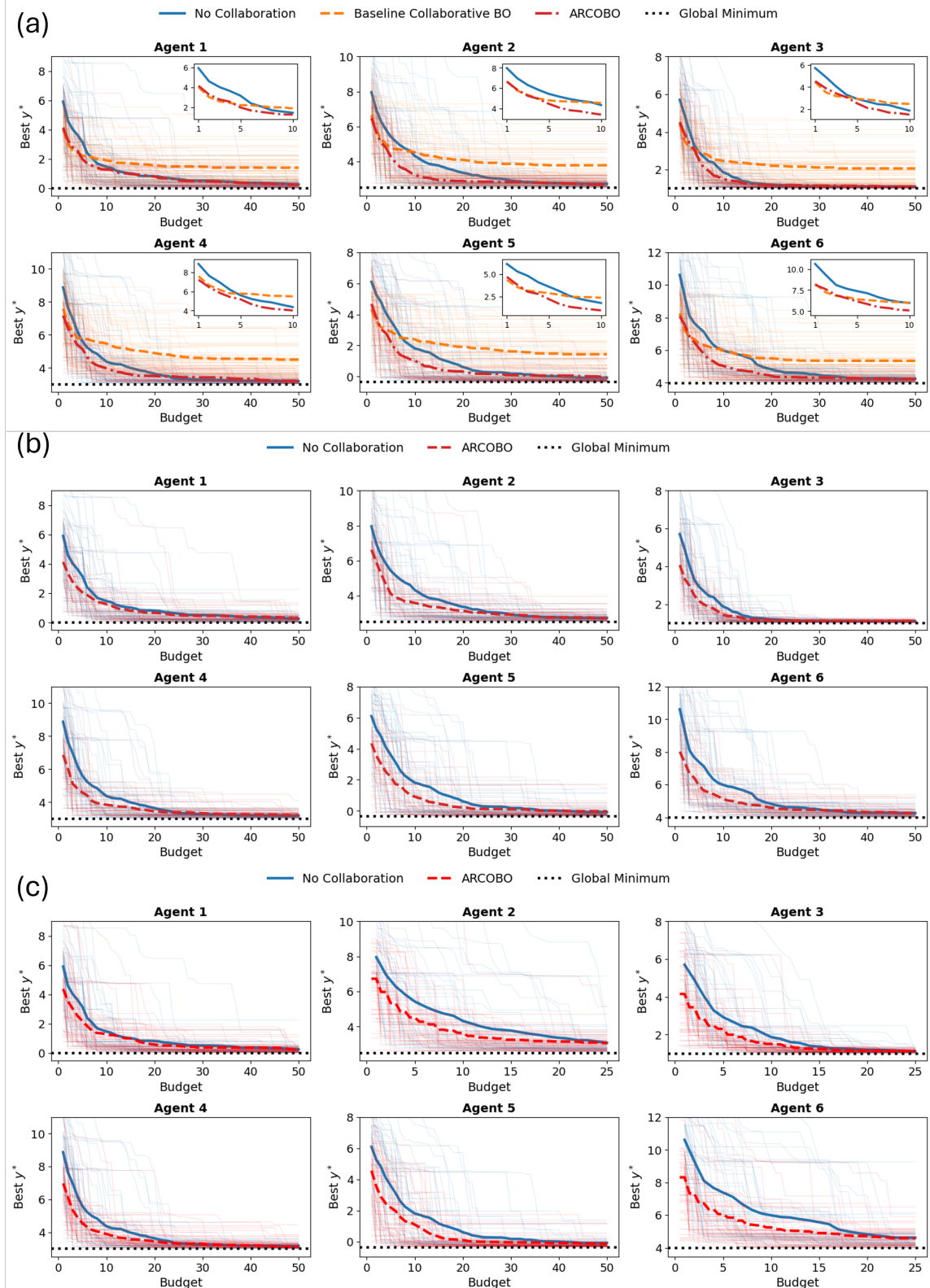


Figure 8: Convergence performance across 50 replicates for ARCO-BO and separate BO on the multi-agent Ackley problem with (a) same budgets and fully shareable input, (b) different budgets for each agents, (c) different shareable inputs.

lacks collaborative benefits.

Overall, these results demonstrate that ARCO-BO's adaptive collaboration strategy works with varying input sharing constraints and resource heterogeneity. It provides an

505

506

507

efficient optimization framework for scenarios where traditional BO frameworks struggle due to limited budgets or incomplete information sharing. 508
509

5.3 Example on High-Dimensional Engineering Benchmarks 510

We performed 20 independent replicates for both the Borehole and Wing Weight problems under a multi-agent setting. These two functions are both modified from [2]. The results are summarized in Table 3 and visualized in Fig. 9. In each benchmark, agents operate under different evaluation budgets, and only a subset of the input space is shared across agents. Full specifications of the agent-specific functions, budget allocations, and shared input dimensions are provided in Table A3 and Table A4. 511
512
513
514
515
516

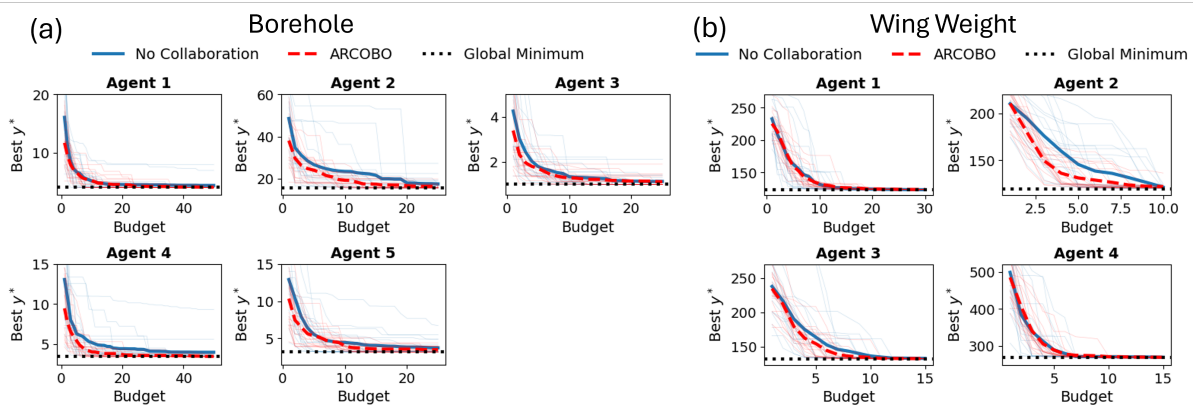


Figure 9: Convergence performance across 20 replicates for ARCO-BO and separate BO on the (a) Borehole problem, and (b) Wing Weight problem.

Across both benchmark problems, ARCO-BO consistently outperforms separate BO in terms of both early convergence and final solution quality, as shown in Table 3. Figure 9a illustrates these gains on the Borehole benchmark. For example, Agents 2, 3, and 5 operate under reduced evaluation budgets, which would typically limit their ability to reach the global optimum. However, with ARCO-BO, these agents are able to benefit from collaborative information sharing with higher-budget peers, allowing them to converge effectively despite fewer evaluations. A similar trend is observed in Figure 9b for the Wing Weight benchmark, particularly for Agent 2 where ARCO-BO shows significant improvement over separate BO. Without collaboration, the agent lacks sufficient information to escape poor regions of the design space. ARCO-BO, by contrast, enables faster convergence by leveraging inter-agent knowledge to guide optimization across heterogeneous settings. 517
518
519
520
521
522
523
524
525
526
527
528

The superior performance of ARCO-BO across these engineering benchmarks stems from its ability to adaptively coordinate learning across heterogeneous agents. Using similarity-aware consensus, it avoids negative transfer from dissimilar tasks, which improves convergence. Its budget-aware asynchronous sampling helps agents with limited evaluations allocate resources more effectively. Partial input space sharing enables collaboration even when agents operate on different subsets of the design space. Together, these 529
530
531
532
533
534

mechanisms let ARCO-BO exploit complementary information, increase sample efficiency, 535 and deliver consistently better solutions than independent BO in complex multi-agent set- 536 tings. 537

Table 3: Normalized AUC and final regrets for Borehole and Wing Weight problems (mean \pm std over 20 replicates).

Benchmark	Method	AUC	Final Regret
Borehole	Separate BO	0.0251 ± 0.0178	0.0018 ± 0.0038
	ARCO-BO	0.0174 ± 0.0101	0.0008 ± 0.0016
Wing Weight	Separate BO	0.0807 ± 0.0757	0.0274 ± 0.0576
	ARCO-BO	0.0471 ± 0.0188	0.0026 ± 0.0050

6. Conclusion

This work introduces ARCO-BO, a framework for multi-agent BO in heterogeneous set- 539 tings. ARCO-BO addresses key challenges such as task heterogeneity, resource disparity, 540 and partially shared input spaces, which are common in real-world collaborative scenarios 541 such as distributed manufacturing, material discovery, and multi-fidelity design. The pro- 542 posed framework integrates three core innovations to enable effective collaboration: 543

- Similarity and optima-aware consensus mechanisms that adaptively regulate inter- 544 agent influence based on surrogate model alignment. 545
- A budget-aware sampling strategy that allocates evaluations according to each 546 agent’s available resources. 547
- A strategy to handle partially shared inputs that enables collaboration while pre- 548 serving private design variables. 549

Experiments on synthetic problems and engineering benchmarks show that ARCO- 550 BO consistently outperforms independent BO and conventional collaborative BO via 551 consensus. It converges faster and achieves lower regret under heterogeneous budgets and 552 partially shared inputs, with low-budget agents gaining from targeted knowledge transfer 553 by high-budget peers without being misled by irrelevant information. 554

These gains stem from ARCO-BO’s distinctive approach to information sharing, which 555 sets it apart from existing multi-agent design strategies. Consensus-based collaborative 556 BO methods coordinate decisions while avoiding raw data exchange, but their reliance on 557 uniform averaging often ignores task heterogeneity and budget asymmetry. At the other 558 extreme, multi-source data fusion methods combine all agents’ input–output data into a 559 unified surrogate, but require full data sharing and degrade in performance under strong 560 heterogeneity or privacy constraints. 561

Despite its advantages, ARCO-BO still assumes fixed evaluation budgets and depends on user-defined hyperparameters, such as the consensus decay rate, which may limit its adaptability in dynamic environments. Future extensions could incorporate adaptive budgeting strategies, self-tuning consensus mechanisms, and dynamic agent participation, as well as support for richer forms of input heterogeneity, including mixed discrete-continuous domains and agent-specific constraints. Beyond addressing these limitations, ARCO-BO also opens broader opportunities. Its emphasis on selective and resource-aware collaboration aligns naturally with settings where data sharing is constrained and evaluations are expensive, such as federated optimization, cooperative scientific design, and distributed engineering. Reinforcement learning offers another promising direction, where consensus updates could themselves be adapted through learned policies that regulate inter-agent influence over time, guide sampling with a long-term view of performance.

A. Details of Test Functions

This section presents detailed formulations and configurations for all benchmark functions used in our study. These include two illustrative examples—a 1D Sasena function (Table A1) and a 2D multi-fidelity Ackley function (Table A2), as well as two engineering-inspired high-dimensional problems: the Borehole (Table A3) and Wing Weight (Table A4) functions. For each case, we specify the agent-specific modifications, input bounds, sample budgets, and known optima. These functions collectively span a range of heterogeneities in input dimension, fidelity structure, and inter-agent similarity, serving to rigorously evaluate the proposed optimization framework.

Table A1: 1D illustrative example: Sasena function. Formulation, upper/lower bounds, initial sample size, budget, and true optimal value of each agent.

Agent	Formulation	Upper/lower bound	Init. Sample	Budget	True optimal	op-
1	$y_1(x) = -\sin x - \exp\left(\frac{x}{10}\right) + 10$	$0 \leq x \leq 10$	3	20	6.782	
2	$y_2(x) = -\sin(0.95x) - \exp\left(\frac{x}{50}\right) + 0.03(x-2)^2 + 10.3$		3	20	8.269	
3	$y_3(x) = -\sin(0.8x) - \exp\left(\frac{x}{50}\right) + 0.03(x-2)^2 + 8$		3	20	5.959	

References

[1] T. Kvan, Collaborative design: What is it? *Automation in construction*, vol. 9, no. 4, pp. 409–415, 2000.

[2] Y.-P. Chen, L. Wang, Y. Comlek and W. Chen, A latent variable approach for non-hierarchical multi-fidelity adaptive sampling, *Computer Methods in Applied Mechanics and Engineering*, vol. 421, p. 116 773, 2024. 586
587
588

[3] M. M. Noack and J. A. Sethian, ‘Autonomous discovery in science and engineering,’ *USDOE Office of Science (SC)(United States)*, Tech. Rep., 2021. 589
590

[4] D. Khatamsaz, J. Wagner, B. Vela, R. Arroyave and D. L. Allaire, Towards autonomous experimentation: Bayesian optimization over problem formulation space for accelerated alloy development, *arXiv preprint arXiv:2502.05735*, 2025. 591
592
593

[5] C. W. Coley, N. S. Eyke and K. F. Jensen, Autonomous discovery in the chemical sciences part i: Progress, *Angewandte Chemie International Edition*, vol. 59, no. 51, pp. 22 858–22 893, 2020. 594
595
596

[6] R. Kontar, N. Shi, X. Yue, S. Chung, E. Byon, M. Chowdhury, J. Jin, W. Kontar, N. Masoud, M. Nouiehed et al., The internet of federated things (ioft), *IEEE Access*, vol. 9, pp. 156 071–156 113, 2021. 597
598
599

[7] Y. Liu, X. Yue, J. Zhang, Z. Zhai, A. Moammeri, K. J. Edgar, A. S. Berahas, R. Al Kontar and B. N. Johnson, Scalable accelerated materials discovery of sustainable polysaccharide-based hydrogels by autonomous experimentation and collaborative learning, *ACS Applied Materials & Interfaces*, vol. 16, no. 51, pp. 70 310–70 321, 2024. 600
601
602
603
604

[8] X. Yue, Y. Liu, A. S. Berahas, B. N. Johnson and R. Al Kontar, Collaborative and distributed bayesian optimization via consensus, *IEEE Transactions on Automation Science and Engineering*, 2025. 605
606
607

[9] J. Juziuk, D. Weyns and T. Holvoet, Design patterns for multi-agent systems: A systematic literature review, in *Agent-Oriented Software Engineering*, Springer, 2014, pp. 79–99. 608
609
610

[10] S. A. DeLoach and M. Kumar, Multi-agent systems engineering: An overview and case study, *Agent-oriented methodologies*, pp. 317–340, 2005. 611
612

[11] T. Yang, X. Yi, J. Wu, Y. Yuan, D. Wu, Z. Meng, Y. Hong, H. Wang, Z. Lin and K. H. Johansson, A survey of distributed optimization, *Annual Reviews in Control*, vol. 47, pp. 278–305, 2019. 613
614
615

[12] T.-H. Chang, M. Hong and X. Wang, Multi-agent distributed optimization via inexact consensus admm, *IEEE Transactions on Signal Processing*, vol. 63, no. 2, pp. 482–497, 2014. 616
617
618

[13] A. Nedic and A. Ozdaglar, Distributed subgradient methods for multi-agent optimization, *IEEE Transactions on automatic control*, vol. 54, no. 1, pp. 48–61, 2009. 619
620

[14] A. Amirkhani and A. H. Barshooyi, Consensus in multi-agent systems: A review, *Artificial Intelligence Review*, vol. 55, no. 5, pp. 3897–3935, 2022. 621
622

[15] J. Qin, Q. Ma, Y. Shi and L. Wang, Recent advances in consensus of multi-agent systems: A brief survey, *IEEE Transactions on Industrial Electronics*, vol. 64, no. 6, pp. 4972–4983, 2016. 623
624
625

[16] Y. Li and C. Tan, A survey of the consensus for multi-agent systems, *Systems Science & Control Engineering*, vol. 7, no. 1, pp. 468–482, 2019. 626
627

[17] R. Olfati-Saber, J. A. Fax and R. M. Murray, Consensus and cooperation in networked multi-agent systems, *Proceedings of the IEEE*, vol. 95, no. 1, pp. 215–233, 2007. 628
629
630

[18] E. Semsar-Kazerooni and K. Khorasani, Multi-agent team cooperation: A game theory approach, *Automatica*, vol. 45, no. 10, pp. 2205–2213, 2009. 631
632

[19] G. Boella and L. VAN DER TORRE, A game-theoretic approach to normative multi-agent systems, *Normative Multi-agent Systems*, 2007. 633
634

[20] M. Niazi and A. Hussain, Agent-based computing from multi-agent systems to agent-based models: A visual survey, *Scientometrics*, vol. 89, no. 2, pp. 479–499, 2011. 635
636
637

[21] R. C. Cardoso and A. Ferrando, A review of agent-based programming for multi-agent systems, *Computers*, vol. 10, no. 2, p. 16, 2021. 638
639

[22] L. Canese, G. C. Cardarilli, L. Di Nunzio, R. Fazzolari, D. Giardino, M. Re and S. Spanò, Multi-agent reinforcement learning: A review of challenges and applications, *Applied Sciences*, vol. 11, no. 11, p. 4948, 2021. 640
641
642

[23] L. Buşoniu, R. Babuška and B. De Schutter, Multi-agent reinforcement learning: An overview, *Innovations in multi-agent systems and applications-1*, pp. 183–221, 2010. 643
644
645

[24] K. Zhang, Z. Yang and T. Başar, Multi-agent reinforcement learning: A selective overview of theories and algorithms, *Handbook of reinforcement learning and control*, pp. 321–384, 2021. 646
647
648

[25] I. Gligore, M. Cioca, R. Oancea, A.-T. Gorski, H. Gorski and P. Tudorache, Adaptive learning using artificial intelligence in e-learning: A literature review, *Education Sciences*, vol. 13, no. 12, p. 1216, 2023. 649
650
651

[26] F. Martin, Y. Chen, R. L. Moore and C. D. Westine, Systematic review of adaptive learning research designs, context, strategies, and technologies from 2009 to 2018, *Educational Technology Research and Development*, vol. 68, no. 4, pp. 1903–1929, 2020. 652
653
654
655

[27] P. I. Frazier, A tutorial on bayesian optimization, *arXiv preprint arXiv:1807.02811*, 2018. 656
657

[28] M. Pelikan and M. Pelikan, *Hierarchical Bayesian optimization algorithm*. Springer, 2005. 658
659

[29] P. I. Frazier, Bayesian optimization, in *Recent advances in optimization and modeling of contemporary problems*, Informs, 2018, pp. 255–278. 660
661

[30] M. Seeger, Gaussian processes for machine learning, *International journal of neural systems*, vol. 14, no. 02, pp. 69–106, 2004. 662
663

[31] Q. Chen, L. Jiang, H. Qin and R. A. Kontar, Multi-agent collaborative bayesian optimization via constrained gaussian processes, *Technometrics*, vol. 67, no. 1, pp. 32–45, 2025. 664
665
666

[32] D. Zhan, H. Zhang, R. Righter, Z. Zheng and J. Anderson, Collaborative bayesian optimization via wasserstein barycenters, *arXiv preprint arXiv:2504.10770*, 2025. 667
668

[33] S. K. Ravi, Y. Comlek, A. Pathak, V. Gupta, R. Umretiya, A. Hoffman, G. Pilania, P. Pandita, S. Ghosh, N. Mckeever et al., Interpretable multi-source data fusion through latent variable gaussian process, *Engineering Applications of Artificial Intelligence*, vol. 145, p. 110 033, 2025. 669
670
671
672

[34] Y. Zhang, S. Tao, W. Chen and D. W. Apley, A latent variable approach to gaussian process modeling with qualitative and quantitative factors, *Technometrics*, vol. 62, no. 3, pp. 291–302, 2020. 673
674
675

[35] Y. Comlek, S. K. Ravi, P. Pandita, S. Ghosh, L. Wang and W. Chen, Heterogenous multi-source data fusion through input mapping and latent variable gaussian process, *Journal of Mechanical Design*, vol. 147, no. 4, p. 041 711, 2025. 676
677
678

[36] R. Al Kontar, Collaborative and federated black-box optimization: A bayesian optimization perspective, in *2024 IEEE International Conference on Big Data (Big-Data)*, IEEE, 2024, pp. 7854–7859. 679
680
681

[37] A. Talapatra, S. Boluki, T. Duong, X. Qian, E. Dougherty and R. Arróyave, Autonomous efficient experiment design for materials discovery with bayesian model averaging, *Physical Review Materials*, vol. 2, no. 11, p. 113 803, 2018. 682
683
684

[38] T. Lookman, P. V. Balachandran, D. Xue and R. Yuan, Active learning in materials science with emphasis on adaptive sampling using uncertainties for targeted design, *npj Computational Materials*, vol. 5, no. 1, p. 21, 2019. 685
686
687

[39] V. Smith, C.-K. Chiang, M. Sanjabi and A. S. Talwalkar, Federated multi-task learning, *Advances in neural information processing systems*, vol. 30, 2017. 688
689

[40] A. G. Kusne and A. McDannald, Scalable multi-agent lab framework for lab optimization, *Matter*, vol. 6, no. 6, pp. 1880–1893, 2023. 690
691

[41] A. D. Zemskov, Y. Fu, R. Li, X. Wang, V. Karkaria, Y.-K. Tsai, W. Chen, J. Zhang, R. Gao, J. Cao et al., Security and privacy of digital twins for advanced manufacturing: A survey, *arXiv preprint arXiv:2412.13939*, 2024. 692
693
694

[42] J. Schmidt, M. R. Marques, S. Botti and M. A. Marques, Recent advances and applications of machine learning in solid-state materials science, *npj computational materials*, vol. 5, no. 1, p. 83, 2019. 695
696
697

[43] B. Shahriari, K. Swersky, Z. Wang, R. P. Adams and N. De Freitas, Taking the human out of the loop: A review of bayesian optimization, *Proceedings of the IEEE*, vol. 104, no. 1, pp. 148–175, 2015. 698
699
700

[44] J. Mockus, The bayesian approach to global optimization, in *System Modeling and Optimization: Proceedings of the 10th IFIP Conference New York City, USA, August 31–September 4, 1981*, Springer, 2005, pp. 473–481. 701
702
703

[45] J. Močkus, On bayesian methods for seeking the extremum, in *Optimization Techniques IFIP Technical Conference Novosibirsk, July 1–7, 1974* 6, Springer, 1975, pp. 400–404. 704
705
706

[46] J. Snoek, H. Larochelle and R. P. Adams, Practical bayesian optimization of machine learning algorithms, *Advances in neural information processing systems*, vol. 25, 2012. 707
708
709

[47] Z. Wang, F. Hutter, M. Zoghi, D. Matheson and N. De Feitas, Bayesian optimization in a billion dimensions via random embeddings, *Journal of Artificial Intelligence Research*, vol. 55, pp. 361–387, 2016. 710
711
712

[48] A. Forrester, A. Sobester and A. Keane, *Engineering design via surrogate modelling: a practical guide*. John Wiley & Sons, 2008. 713
714

[49] R. Sinkhorn, A relationship between arbitrary positive matrices and doubly stochastic matrices, *The annals of mathematical statistics*, vol. 35, no. 2, pp. 876–879, 1964. 715
716

[50] A. Grosnit, A. I. Cowen-Rivers, R. Tutunov, R.-R. Griffiths, J. Wang and H. Bou-Ammar, Are we forgetting about compositional optimisers in bayesian optimisation? *Journal of Machine Learning Research*, vol. 22, no. 160, pp. 1–78, 2021. 717
718
719

[51] Z. Xie and L. Chen, Merge kernel for bayesian optimization on permutation space, *arXiv preprint arXiv:2507.13263*, 2025. 720
721

[52] Q. Lin, L. Gong, Y. Zhang, M. Kou and Q. Zhou, A probability of improvement-based multi-fidelity robust optimization approach for aerospace products design, *Aerospace Science and Technology*, vol. 128, p. 107 764, 2022. 722
723
724

[53] D. Ackley, A connectionist machine for genetic hillclimbing. vol. 28, 2012. 725

Table A2: 2D illustrative example: Multi-fidelity Ackley function. Formulation, bounds, initial sample size, budget, and true optimal value (illustrative) for each fidelity level.

Agent	Formulation	Upper/loWat. bound	Sample	Budget	True optimal
1	$y_0(x) = -20 \exp \left(-0.2 \sqrt{0.5 \sum x_i^2} \right)$ $- \exp \left(0.5 \sum \cos(\pi x_i) \right) + 20 + e$	$-5 \leq$ $x_i \leq 5$	5	50	0.000
2	$y_1(x) = -20 \exp \left(-0.2 \sqrt{0.5 \sum (x_i + 0.2)^2} \right)$ $- \exp \left(0.5 \sum \cos(1.1\pi(x_i + 0.2)) \right) + 20 + e + 2.5$	5	50	2.500	
3	$y_2(x) = -20 \exp \left(-0.2 \sqrt{0.5 \sum (0.8(x_i - 0.3))^2} \right)$ $- \exp \left(0.5 \sum \cos(0.9\pi \cdot 0.8(x_i - 0.3)) \right) + 20 + e + 1.0$	5	50/25	1.000	
4	$y_3(x) = -20 \exp \left(-0.2 \sqrt{(x_1 + 0.4)^2} \right)$ $- \exp \left(\cos(\pi(x_1 + 0.4)) \right) + 20 + e + 3.0$	5	50/25	3.000	
5	$y_4(x) = -20 \exp \left(-0.2 \sqrt{0.5 \sum (x_i - 0.5)^2} \right)$ $- 1.5 \exp \left(0.5 \sum \cos(\pi(x_i - 0.5)) \right) + 20 + e + 1.0$	5	50	-0.359	
6	$y_5(x) = 1.1 \left[-20 \exp \left(-0.2 \sqrt{0.5 \sum (x_i - 0.1)^2} \right) \right.$ $\left. - \exp \left(0.5 \sum \cos(\pi(x_i - 0.1)) \right) + 20 + e \right]$ $+ 4.0$	5	50/25	3.978	

Table A3: Borehole function with five agents. Each agent is assigned a modified variant of the borehole function. Variable bounds, shareable inputs, initial sample size, budget, and true optimal value are listed.

Agent	Formulation	Variable Bounds	Shareable init. Inputs	Sample	Budget	True	Optimal
1	$y_1(\mathbf{x}) = \frac{2\pi T_u (H_u - H_l)}{\ln(r/r_w) \left(1 + \frac{2LT_u}{r_w^2 K_w \ln(r/r_w)} + \frac{T_u}{T_l} \right)}$	$0.05 \leq r_w \leq r_w$	8	50	3.985		
2	$y_2(\mathbf{x}) = \frac{2\pi T_u (H_u - 0.8H_l)}{\ln(r/r_w) \left(1 + \frac{LT_u}{r_w^2 K_w \ln(r/r_w)} + \frac{T_u}{T_l} \right)}$	$0.15 \leq r_w \leq T_u$	8	25	15.582		
3	$y_3(\mathbf{x}) = \frac{2\pi T_u (H_u - H_l)}{\ln(r/r_w) \left(1 + \frac{8LT_u}{r_w^2 K_w \ln(r/r_w)} + 0.75 \frac{T_u}{T_l} \right)}$	$100 \leq r \leq 10000$	$H_u \leq T_l \leq T_u$	8	25	1.000	
4	$y_4(\mathbf{x}) = \frac{2\pi T_u (1.09 H_u - H_l)}{\ln(4r/r_w) \left(1 + \frac{3LT_u}{r_w^2 K_w \ln(r/r_w)} + \frac{T_u}{T_l} \right)}$	$10 \leq T_l \leq 500$	$700 \leq H_l \leq 820$	8	50	3.434	
5	$y_5(\mathbf{x}) = \frac{2\pi T_u (1.05 H_u - H_l)}{\ln(2r/r_w) \left(1 + \frac{3LT_u}{r_w^2 K_w \ln(r/r_w)} + \frac{T_u}{T_l} \right)}$	$L \leq K_w \leq 12000$	8	25	3.153		

Table A4: Wing weight function with four agents. Each agent is assigned a modified variant of the wing weight function. Variable bounds, shareable inputs, initial sample size, budget, and true optimal value are listed.

Agent	Formulation	Variable Bounds	Shareable Inputs	Init. Sample	Budget	True Optimal
1	$y_1(\mathbf{x}) = 0.036 s_w^{0.758} w_{fw}^{0.0035} \left(\frac{A}{\cos^2(\Lambda)} \right)^{0.6}$			5	30	123.25
	$q^{0.006} \lambda^{0.04} \left(\frac{100 t_c}{\cos(\Lambda)} \right)^{-0.3} ((N_z W_{dg})^{0.49} + s_w w_{fw}^{0.3}) \leq s_w \leq 200$					
2	$y_2(\mathbf{x}) = 0.036 s_w^{0.758} w_{fw}^{0.0035} \left(\frac{A}{\cos^2(\Lambda)} \right)^{0.6}$	$220 \leq w_{fw} \leq 300$	w_{fw}	5	10	119.53
	$q^{0.006} \lambda^{0.04} \left(\frac{100 t_c}{\cos(\Lambda)} \right)^{-0.3} ((N_z W_{dg})^{0.49} + w_p)^{-1} 10 \leq \Lambda \leq 10$	$6 \leq A \leq 10$	A			
3	$y_3(\mathbf{x}) = 0.036 s_w^{0.758} w_{fw}^{0.0035} \left(\frac{A}{\cos^2(\Lambda)} \right)^{0.6}$	$16 \leq q \leq 45$	q	5	20	131.65
	$q^{0.005} \lambda^{0.04} \left(\frac{100 t_c}{\cos(\Lambda)} \right)^{-0.3} ((N_z W_{dg})^{0.49} + w_p)^{-1} 0.08 \leq t_c \leq 0.18$	$0.5 \leq \lambda \leq 1$				
4	$y_4(\mathbf{x}) = 0.036 s_w^{0.9} w_{fw}^{0.0035} \left(\frac{A}{\cos^2(\Lambda)} \right)^{0.6}$	$1700 \leq W_{dg} \leq 2500$	W_{dg}	5	20	268.13
	$q^{0.005} \lambda^{0.04} \left(\frac{100 t_c}{\cos(\Lambda)} \right)^{-0.3} (N_z W_{dg})^{0.49}$	$0.025 \leq w_p \leq 0.08$				